# A Novel Directional Pilot Protection Method for EHV Transmission Lines Considering Fault Factors

Zhenwei Guo, Yingcai Deng, Ruiqiang Zhao, Tong Zhang

*Abstract*—**The traveling wave directional protection offers the advantage of ultra-high-speed action and high sensitivity, meeting the urgent demand for high-speed protection in extra-high-voltage (EHV) transmission systems. However, conventional traveling wave directional protection exhibits insufficient reliability during weak faults, i.e., large fault resistance and small fault angles, making it challenging to implement in reality. Based on the energy difference between reverse and forward traveling waves, this paper proposes a novel traveling wave directional pilot protection method considering fault factors. The method identifies the fault direction using the Normalised Directional Energy Difference (NED). The NED is greater than the threshold for forward faults and less than the threshold for reverse faults. The NED contains information about the fault resistance and the fault angle, effectively eliminating their influence. Based on the engineering parameters of the Central China Power Grid, a 500 kV transmission system is simulated in EMTP-RV. Extensive test results demonstrate that the proposed method can swiftly and reliably identify fault directions under different fault conditions.**

*Index Terms*— **fault factors, normalized energy, pilot protection, traveling wave, ultra-high-speed**

## I. Introduction

EXTRA-hight-voltage (EHV) transmission lines are characterized by their significant transmission capacity, high transmission efficiency, and low energy losses, making them widely used for large-scale power transmission and the interconnection of asynchronous power grids. In order to ensure the stable operation of power systems and the safety of electrical facilities, reliable detection and rapid fault isolation are becoming increasingly important. [1], [2], [3].

Protection schemes based on voltage and current power frequency information are widely applied in transmission system. However, to obtain post-fault data, the operational time of these protection methods typically exceeds one cycle, failing to meet the requirements for ultra-high-speed protection. The traveling wave (TW) generated by faults contains valuable information, including the type, direction, and location of the fault. The intense demand for ultra-high-speed protection has spurred investigation into TW protection [4]. The propagation speed of TW is comparable to the speed of light, enabling TW protection to achieve the performance of ultra-high-speed action. In addition, unaffected by power system oscillations and current transformer saturation, TW protection is considered an ideal method for safeguarding EHV transmission lines [5], [6], [7], [8]. According to different principles, TW protection is categorized into TW differential protection, TW distance protection, and TW directional protection.

TW direction protection has received a lot of attention because only a small amount of data communication is required to determine the direction of the fault. Reference [9] explored the relationship between voltage increments and current increments, proposing a correlation-based directional relay. The protective method based on this relay avoids the bandwidth limitations of Capacitive Voltage Transformers (CCVTs). Reference [10] utilized the S-transform to extract initial voltage and current TWs and proposed a characteristic impedance directional relay. Based on the differences in transient energy during positive and backward fault occurrences, [11] proposed a novel ultra-high-speed pilot protection. A notable advantage of this protection is its low sampling rate requirement. Using a novel synchronous compressed S-transform to extract fault TW information, [12] investigated the difference in directional TW energy ratios and proposed a transient protection algorithm for AC transmission lines linked to LCC-HVDC inverter stations. Reference [13] proposed a non-unit protection algorithm based on transient current normalization, which extends the protection coverage to twice that of conventional methods. However, a notable drawback of these methods is their failure to consider the impact of fault factors on TW protection. In fact, the reliability of TW protection is often difficult to ensure during faults with high fault resistance and small fault angle, which limits its practical application. To enhance the reliability of TW protection, [14] proposed a distributed unit transient protection method based on machine learning. However, acquiring substantial amounts of data to train Support Vector Machines (SVMs) is still a challenge in practice [15], and this approach does not fundamentally solve the aforementioned problem.

To address the problem of inadequate reliability of TW protection under weak faults conditions, this paper proposes a TW directional pilot protection considering fault factors. Firstly, the difference of forward and backward TW energy after faults is studied, and the basic method for orientation discrimination is derived. Secondly, through extensive

Manuscript received July 20, 2024; revised January 7, 2025.

This research was supported by National Natural Science Foundation of China (No. 52067005) and Guangxi of China Natural Science Foundation (No. 2021GXNSFAA220061).

Zhenwei Guo is an Associate Professor at School of Mechanical and Electrical Engineering, Guilin University of Electronic Technology, Guilin 541000, China. (e-mail: gzwcbf@sina.com).

Yingcai Deng is a postgraduate student at School of Mechanical and Electrical Engineering, Guilin University of Electronic Technology, Guilin 541000, China. (e-mail: d18378392337@163.com).

Ruiqiang Zhao is a postgraduate student at School of Mechanical and Electrical Engineering, Guilin University of Electronic Technology, Guilin 541000, China. (e-mail: 3295657367@qq.com).

Tong Zhang is an Associate Professor at School of Mechanical and Electrical Engineering, Guilin University of Electronic Technology, Guilin 541000, China. (e-mail: mala@guet.edu.cn).

simulation experiments, this paper demonstrates the necessity of considering fault factors in fault discrimination. Thirdly, the protection algorithm considering fault factors is proposed. Finally, we constructed an EMTP-RV simulation model based on the parameters of the Central China Power Grid. Extensive testing results have indicated that this method can reliably determine fault directions under diverse fault conditions, effectively eliminating the influence of fault factors.

## II. Investigation of Traveling Wave Transmission Properties

### A. The EHV Transmission System

Fig. 1 depicts a typical EHV transmission system. The protected object is the MN line, with relays $R_1$ and $R_2$ installed at both terminals. The lengths of the lines LM, MN, and NR are denoted by $l_1$, $l_2$, and $l_3$, respectively. The forward direction refers to the direction from the bus towards the protected transmission line. $F_1$, $F_2$, and $F_3$ represent faults occurring at various locations, where $F_1$ and $F_3$ represent internal faults, and $F_2$ represents external faults.

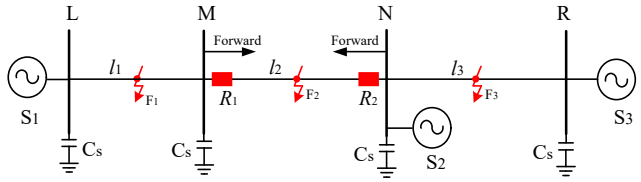


Fig. 1. Structure of the EHV transmission system.

### B. Characteristics of Forward Faults

For convenience, the EHV system shown in Fig. 1 can be considered as a single-phase system. This principle can be conveniently utilized in three-phase systems by converting single-phase signals into line-mode signals [16]. Relay $R_1$ is employed to analyze the energy characteristics of directional TW during faults, and $R_2$ holds the same conclusions as $R_1$.

Suppose that the fault occurs at point $F_2$ in the positive direction of relay $R_1$, which is $x_2$ kilometers away from bus M. The fault-generated TWs propagates in different directions from point $F_2$ and are refracted and reflected at the discontinuity of characteristic impedance. The fault-attached system and TW lattice diagram are drawn in Fig. 2.

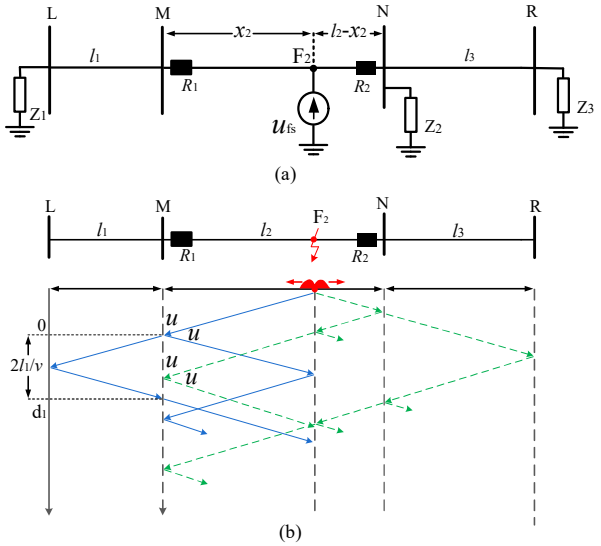


Fig. 2. Fault at point $F_2$. (a) Fault-attached system; (b) TW lattice diagram.

Within the time interval [0, $d_1$], where 0 denotes the moment when the first TW arrives at relay $R_1$, $d_1 = 2l_1/v$, and $v$ represents the speed of the TW, $R_1$ can detect the reverse TWs $u_1^-$ and $u_2^-$, as well as the forward TWs $u_1^+$ and $u_2^+$.

This paper utilizes the integral of the square of transient components to represent the energy of the signal [12], defining the energy of the transient component of the fault voltage as in (1).

$$E = \int_{t_0}^{t_0+d} [\Delta u(t)]^2 \mathrm{d}t \tag{1}$$

where $d$ is the sampling data window.

In this paper, $E_{r1}$ and $E_{f1}$ represent the reverse and forward TW energy detected by $R_1$, respectively. In contrast, $E_{r2}$ and $E_{f2}$ represent the reverse and forward TW energy detected by $R_2$. According to (1) and considering the attenuation of the TW on the transmission line, within the time interval [0, $d_1$], the $E_{r1}$ is as stated in (2).

$$\begin{aligned} E_{r1} &= \int_0^{d_1} \{[u_1^-]^2 + [u_2^-]^2\} \mathrm{d}t \\ &= [\varepsilon^2 x_2^2 + \varepsilon^6 x_2^2 (l_2 - x_2)^4 K_{zf2}^2] \times \int_0^{d_1} u_f^2 \mathrm{d}t \end{aligned} \tag{2}$$

where $\varepsilon$ represents the attenuation coefficient per kilometre of the transmission line, and $K_{zf2}$ denotes the voltage reflection coefficient at point $F_2$.

Within the time interval [0, $d_1$], the $E_{f1}$ is as stated in (3).

$$\begin{aligned} E_{f1} &= \int_0^{d_1} \{[u_1^+]^2 + [u_2^+]^2\} \mathrm{d}t \\ &= [\varepsilon^2 x_2^2 K_{rM}^2 + \varepsilon^6 x_2^2 (l_2 - x_2)^4 K_{zf2}^2 K_{rM}^2] \times \int_0^{d_1} u_f^2 \\ &= K_{rM}^2 \times E_{r1} \end{aligned} \tag{3}$$

where $K_{rM}$ is the voltage reflection coefficient at bus M.

When a fault arises on the NR line at $F_3$, which is $x_3$ kilometers from bus N, the fault-attached system and TW lattice diagram are drawn in Fig. 3.

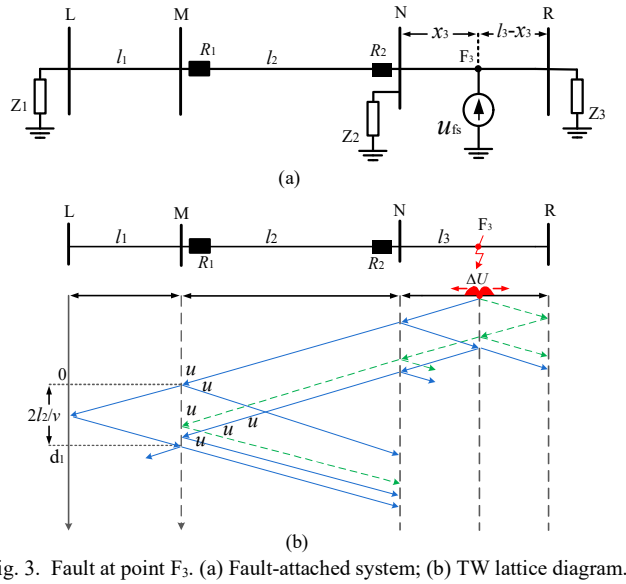


Fig. 3. Fault at point $F_3$. (a) Fault-attached system; (b) TW lattice diagram.

From Fig. 3, it can be observed that when the fault occurs at point $F_3$, within the time interval [0, $d_1$], relay $R_1$ can detect the reverse TWs $u_1^-$, $u_2^-$, and $u_3^-$, as well as the forward TWs $u_1^+$, $u_2^+$, and $u_3^+$.

Within the time interval [0, $d_1$], the $E_{r1}$ is shown as (4).

$$\begin{aligned} E_{r1} &= \int_0^{d_1} \{[u_1^-]^2 + [u_2^-]^2 + [u_3^-]^2\} \mathrm{d}t \\ &= [\varepsilon^4 x_3^2 l_2^2 K_{zN}^2 + \varepsilon^8 x_3^2 (l_3 - x_3)^4 l_2^2 K_{rR}^2 K_{zf3}^2 K_{zN}^2 \\ &\quad + \varepsilon^8 x_3^6 l_2^2 K_{rN}^2 K_{rf3}^2 K_{zN}^2] \times \int_0^{d_1} u_f^2 \mathrm{d}t \end{aligned} \tag{4}$$

where $K_{rR}$, $K_{rN}$, and $K_{rf3}$ denote the voltage reflection coefficients at bus R, bus N, and point $F_3$, respectively, and $K_{zN}$ and $K_{zf3}$ denote the voltage refraction coefficients at bus N and point $F_3$, respectively.

Within the time interval [0, $d_1$], the $E_{f1}$ is shown as (5).

$$\begin{aligned} E_{f1} &= \int_0^{d_1} \{[u_1^+]^2 + [u_2^+]^2 + [u_3^+]^2\} dt \\ &= \varepsilon^4 x_3^2 l_2^2 K_{zN}^2 K_{rM}^2 + \varepsilon^8 x_3^2 (l_3 - x_3)^4 l_2^2 K_{rQ}^2 K_{zf3}^2 K_{zN}^2 K_{rM}^2 \\ &+ \varepsilon^8 x_3^6 l_2^2 K_{rN}^2 K_{rf3}^2 K_{zN}^2 K_{rM}^2] \times \int_0^{d_1} u_f^2 = K_{rM}^2 \times E_{r1} \end{aligned} \tag{5}$$

From (2), (3), (4), and (5), it can be derived that when faults occur in the forward direction of $R_1$:

$$E_{f1} = K_{rM}^2 \times E_{r1} \tag{6}$$

where $-1 < K_{rM} < 1$, thus $E_{f1} < E_{r1}$.

### C. Characteristics of Reverse Fault

When a fault arises on the LM line at $F_1$, which is $x_1$ kilometers from bus M, the fault-attached system and TW lattice diagram are drawn in Fig. 4.

From Fig. 4, it can be observed that when the fault occurs at point $F_1$, within the time interval [0, $d_2$], where $d_2=2l_2/v$, relay $R_1$ can only detect forward TWs $u_1^+$, $u_2^+$, and $u_3^+$.

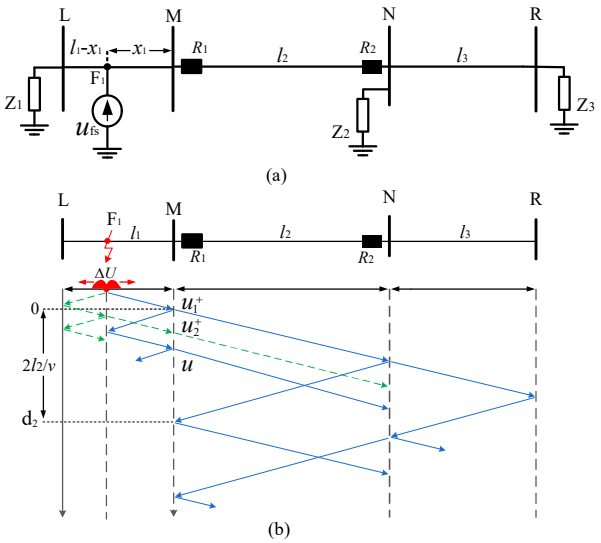


Fig. 4. Fault at point $F_1$. (a) Fault-attached system; (b) TW lattice diagram.

Within the time interval [0, $d_2$], the $E_{f1}$ is as stated in (7).

$$\begin{aligned} E_{f1} &= \int_0^{d_2} \{[u_1^+]^2 + [u_2^+]^2 + [u_3^+]^2\} dt \\ &= [\varepsilon^4 x_1^4 K_{zM}^4 + \varepsilon^6 x_1^2 (l_1 - x_1)^4 K_{rL}^2 K_{zf1}^2 K_{zM}^2 \\ &+ \varepsilon^6 x_1^6 K_{rM}^2 K_{rf1}^2 K_{zM}^2] \times \int_0^{d_2} u_f^2 dt \end{aligned} \tag{7}$$

where $K_{rL}$ and $K_{rf1}$ respectively denote the voltage reflection coefficients at bus L and point $F_1$, and $K_{zf1}$ denotes the voltage refraction coefficient at point $F_1$.

Within the time interval [0, $d_2$], no reverse TW arrives at $R_1$. Thus, the $E_{r1}$ is shown as (8).

$$E_{r1} \approx 0 \tag{8}$$

From (7) and (8), when a reverse fault occurs in relay $R_1$:

$$E_{f1} > E_{r1} \approx 0 \tag{9}$$

## III. Basic Principles and Limitations of Direction Discrimination

Combining the analyses from Sections 2.2 and 2.3, within the time interval $d$, where $d$ = [0, min($2l_1/v$, $2l_2/v$)], the TW energy exhibits the following characteristics.

When a forward fault occurs, $R_1$ simultaneously probes both forward and reverse TWs, satisfying (6). Since $-1 < K_{rM} < 1$, it follows that $E_{r1} > E_{f1}$, thus $E_{r1} - E_{f1} > 0$.

When a reverse fault occurs, no reverse TW reaches $R_1$, satisfying (8). Therefore, $E_{r1} < E_{f1}$, indicating that $E_{r1} - E_{f1} < 0$.

Define $ED_1$ as in (10), representing the fault characteristic of $R_1$. $ED_1 > 0$ indicates a forward fault of $R_1$.

$$ED_1 = E_{r1} - E_{f1} \tag{10}$$

Based on the same principle, define $ED_2$ as in (11), representing the fault characteristic of $R_2$. $ED_2 > 0$ indicates a forward fault of $R_2$, whereas $ED_2 < 0$ indicates a reverse fault of $R_2$.

$$ED_2 = E_{r2} - E_{f2} \tag{11}$$

Therefore, the fundamental principle for determining the direction of faults is:

1) If $ED_1 > 0$ and $ED_2 > 0$, both relays $R_1$ and $R_2$ detect a forward fault, confirming a fault on the MN line.

2) Otherwise, there is no fault on the MN line.

According to the theory above, most faults on the MN lines can be correctly identified. However, further analysis reveals a limitation in the aforementioned principle: the protection does not consider the influence of fault factors. Research indicates that under weak fault conditions, i.e. small fault angles and large fault resistance, the protection may operate incorrectly [17].

Therefore, it is necessary to further improve the above scheme to eliminate the impact of fault factors and enhance the reliability of fault discrimination. Specific schems will be presented in Section 5.

## IV. Impact of Fault Factors

In the system depicted in Fig. 1, when a single-phase ground fault occurs on the MN line, the fault characteristic $ED_1$ of relay $R_1$ varies with fault resistance and fault angle as presented in Fig. 5.

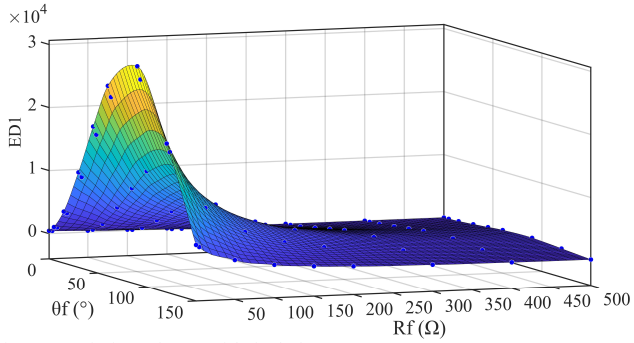


Fig. 5. Variation of $ED_1$ with fault factors.

From the results in Fig. 5, it is evident that fault resistance and fault angle have a significant impact on the fault characteristics. The larger the fault resistance, the smaller the amplitude of $ED_1$. When the fault angle is 90°, the amplitude of $ED_1$ is maximum, whereas it is minimum when the fault angle is 0°. In addition, extensive research suggests that $ED_1$ is a periodic even function of the fault angle, with a symmetry axis at $\theta_f$ = 90°, and a period from 0° to 180°.

Under weak fault conditions, the protection will fail. For instance, when the fault angle is close to 0° and the fault resistance is around 500 Ω, the amplitude of $ED_1$ is nearly 0. Directly using $ED_1$ to determine the fault direction can lead to incorrect judgments. Therefore, the impact of fault resistance

and fault angle must be considered in fault discrimination to enhance the reliability of fault detection.

## V. PROTECTION SCHEME CONSIDERING FAULT FACTORS

### A. S-transform

The continuous wavelet transform (CWT) of the signal $g(t)$ is given by (12) [18], [19].

$$C(\tau, d)=\int_{-\infty}^{\infty} g(t)c(\tau-t,d)\,\mathrm{d}t \tag{12}$$

with $c(\tau-t,d)$ denoting the fundamental wavelet, $d$ representing the scale factor, and $\tau$ indicating the translation factor [20].

The S-transform of the signal $g(t)$ is shown in (13).

$$S(\tau,f)=e^{i2\pi f\tau}C(\tau,d) \tag{13}$$

where $f$ represents the frequency and $i$ denotes the imaginary number. By substituting (12) into (13), the S-transform of $g(t)$ is given as follows [21]:

$$S(\tau,f)=\int_{-\infty}^{\infty} g(t)c(\tau-t,f)e^{-i2\pi ft}\,\mathrm{d}t \tag{14}$$

$$c(\tau-t,f)=\frac{|f|}{\sqrt{2\pi}}\exp^{-\frac{f^2(\tau-t)^2}{2}} \tag{15}$$

where $c(\tau-t,f)$ is the Gaussian window function [22].

Let $g$[kT] (k= 0, 1, 2,..., N-1) be the discrete time series of the time-varying signal $g(t)$. Here, N is the sum of sampling points, and T is the sampling interval. The discrete Fourier transform of $g$[kT] is denoted as X[n/NT], and then the discrete S-transform is shown in (16) and (17).

$$S[kT,\frac{n}{NT}]=\sum_{m=0}^{N-1} G[\frac{m+n}{NT}]e^{-2\pi^2m^2/n^2+i2\pi mk/N},\quad n\neq 0 \tag{16}$$

$$S[kT,0]=\frac{1}{N}\sum_{m=0}^{N-1} g(\frac{m}{NT}),\quad n=0 \tag{17}$$

The result of the S-transform of the discrete time series $g$[kT] is a complex time-frequency matrix, expressed as the S-matrix $S_i[kT,\frac{n}{NT}]$. The S-transform energy at frequency $f_i$ is defined as shown in (18).

$$E_{in}=\sum_{kT}(S_i[kT,\frac{n}{NT}])^2 \tag{18}$$

The total transient energy of the signal at each frequency point is presented in (19).

$$E_n=\sum_i\sum_{kT}(S_i[kT,\frac{n}{NT}])^2=\sum_i E_{in} \tag{19}$$

The S-transform avoids the selection of the mother wavelet in the wavelet transform, and provides superior time-frequency localisation capability to extract the characteristics of transient signals at various frequency efficiently. Given that the S-transform energy in (19) effectively characterizes the energy of the TW in each frequency band, the proposed protection algorithm utilizes S-transform energy to extract the energy of fault-generated TW.

### B. Proposed Protection Algorithm

In order to eliminate the influence of fault factors, the algorithm in this paper normalizes $ED_1$ and $ED_2$ to $NED_1$ and $NED_2$, based on fault resistance and fault angle. The pertinent equations are presented in (20) and (21). Since $NED_1$ and $NED_2$ incorporate information about fault resistance and fault angle, using them to establish directional criteria can eliminate the impact of fault resistance and fault angle, thus improving the reliability of relay directional discrimination.

$$\mathrm{NED}_1=\frac{1}{\lambda}\mathrm{ED}_1 \tag{20}$$

$$\mathrm{NED}_2=\frac{1}{\lambda}\mathrm{ED}_2 \tag{21}$$

where $\lambda$ represents the normalization coefficient, and its mathematical expression is given by (22).

$$\lambda=fit(R_f,\theta_f,ED,'Biharmonic') \tag{22}$$

where $R_f$ represents the fault resistance and $\theta_f$ represents the fault angle.

Therefore, the principle of improved directional pilot protection is:

1) If $NED_1 > \lambda_{set}$ and $NED_2 > \lambda_{set}$, indicating that relays $R_1$ and $R_2$ have detected a forward fault, an internal fault in the MN line is confirmed.

2) Otherwise, there is no fault on the MN line.

To avoid disturbances such as sampling anomalies, the threshold $\lambda_{set}$ should be set with some margin. Combined with simulation tests, in this algorithm, $\lambda_{set}$ is set to 1500.

The directional pilot protection scheme considering fault factors is shown in Fig. 6.

The protection is triggered when the protection device detects a fault TW. At first, the fault voltage and current signals are sampled within a short data window. The phase-mode transform is applied to eliminate the coupling relationships among the three-phase signals, as illustrated in (23).

$$\begin{bmatrix} M_0 \\ M_\alpha \\ M_\beta \\ M_\gamma \end{bmatrix}=\frac{1}{3}\begin{bmatrix} 1 & 1 & 1 \\ 1 & -1 & 0 \\ 1 & 0 & -1 \\ 0 & 1 & -1 \end{bmatrix}\begin{bmatrix} M_a \\ M_b \\ M_c \end{bmatrix} \tag{23}$$

where $M_a$, $M_b$, and $M_c$ represent the three phase voltages or currents. $M_\alpha$, $M_\beta$, and $M_\gamma$ denote the three line-mode components and $M_0$ signifies the zero-mode component. The computational equations for forward and reverse TWs are shown in (24) and (25), respectively. Given that the line-mode components possesses the advantages of fast propagation speed and small attenuation, the algorithm calculates the directional TW using the α mode voltage and current components.

$$\Delta u_{\mathrm{f}}(t)=\frac{1}{2}[\Delta u(t)+Z_c\Delta i(t)] \tag{24}$$

$$\Delta u_{\mathrm{r}}(t)=\frac{1}{2}[\Delta u(t)-Z_c\Delta i(t)] \tag{25}$$

Secondly, the TW transient information is characterized by the S-transform, and the S-transform energies of the forward and reverse TWs are calculated using (19). Subsequently, $ED_1$ and $ED_2$ are calculated separately using (10) and (11).

Finally, based on fault resistance and fault angle, $ED_1$ and $ED_2$ are normalized to $NED_1$ and $NED_2$ respectively. The relevant formulas are given by (20) and (21). Relays $R_1$ and $R_2$ can determine the fault direction based on $NED_1$ and $NED_2$, respectively. The results of fault determination are exchanged through communication channels. If both $R_1$ and $R_2$ detect a fault in the forward direction, i.e. $NED_1 > \lambda_{set}$ and $NED_2 > \lambda_{set}$, an internal fault on the MN line can be confirmed. Otherwise, it is an external fault.

### C. Calculation of Fault Angle

Reference [23] proposed an impedance-based fault

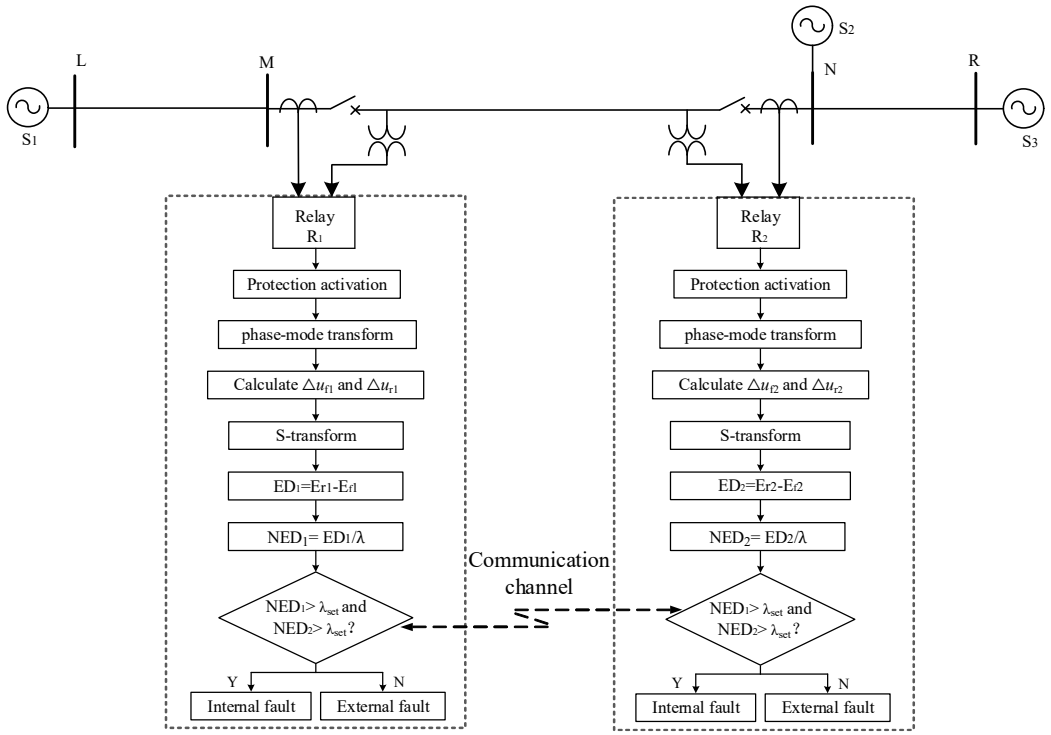


Fig. 6. Scheme of the TW-based directional pilot protection.

location method for transmission lines. The mathematical formula utilizes a generalized equation to calculate the fault distance, and the calculated results are independent of the fault type. The proposed protection algorithm in this paper calculates the fault angle based on fault distance measurement, with a maximum computation error of 0.25%. The accuracy meets the requirements of this algorithm.

### *D. Calculation of Fault Resistance*

In [24], a practical method based on fault record data was proposed for calculating fault resistance on transmission lines. In this paper, we applied this method to calculate the fault resistance with an error of less than 5%, meeting the accuracy requirements of this paper.

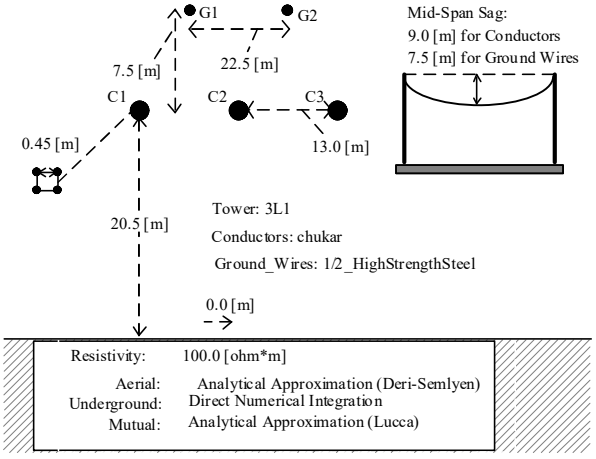


Fig. 7. Configuration of the MN line.

## VI. SIMULATION AND ANALYSIS

### *A. Simulation System and Parameters*

Based on the engineering parameters of the Pingwu project of Central China Power Grid, the transmission system presented in Fig. 1 was constructed in EMTP-RV. The transmission lines utilize frequency-dependent models. The lengths of lines LM, MN, and NR are 150 kilometers, 180 kilometers, and 120 kilometers, respectively. The parameters of Source 1 are $V_{S1} = 525\angle 23.8°$, $Z_{S11} = 0.635 + j7.258$ Ω, $Z_{S10} = 1.674 + j18.565$ Ω. The parameters of Source 2 are $V_{S2} = 525\angle -16.2°$, $Z_{S21} = 0.861+j10.378$ Ω, $Z_{S20} = 2.563 + j25.526$ Ω. The parameters of Source 3 are $V_{S3} = 525\angle 37.4°$, $Z_{S31} = 0.545 + j8.612$ Ω, $Z_{S30} = 1.973 + j19.462$ Ω. The equivalent capacitance to ground for all buses is 0.01 μF [25]. The protected object is the MN line, with its parameters depicted in Fig. 7. The signal sampling rate is 200 kHz, and the data window $d$ is 0.8 ms ($d < 2l_1$/c, $2l_2$/c, and $2l_3$/c).

### *B. Testing of Typical Faults*

The fault resistance is 5 Ω, and the fault angle is 60°. A phase-to-ground fault of phase A was simulated 60 kilometers from bus M on the MN line. The fault-generated directional TW detected by relays $R_1$ and $R_2$ is shown in Fig. 8. As shown in Fig. 8, relays $R_1$ and $R_2$ simultaneously detected both forward and reverse TWs. Further calculations show that for relay $R_1$, $NED_1 = 14666$ and $NED_1 > \lambda_{set}$, indicating that $R_1$ identifies a forward fault. For relay $R_2$, $NED_2 = 6023$ and $NED_2 > \lambda_{set}$, indicating that $R_2$ identifies a forward fault. Combining the discrimination of relays $R_1$ and $R_2$, it is confirmed that there is an internal fault on the MN line, and the fault is correctly identified.

The fault resistance is 5 Ω, and the fault angle is 60°. A phase-to-ground fault of phase A was simulated 80 kilometers from bus N on the NR line. The fault-generated directional TW detected by relays $R_1$ and $R_2$ is shown in Fig. 9. As shown in Fig. 9, relay $R_1$ detected both forward and reverse TWs simultaneously, whereas relay $R_2$ initially detected only the forward TW. Further calculations show that for relay $R_1$, $NED_1 = 4583$ and $NED_1 > \lambda_{set}$, indicating that $R_1$ identifies a forward fault. For relay $R_2$, $NED_2 = -10026$ and $NED_2 < \lambda_{set}$, indicating that $R_2$ identifies a reverse fault. Therefore, it is correctly identified as an external fault.

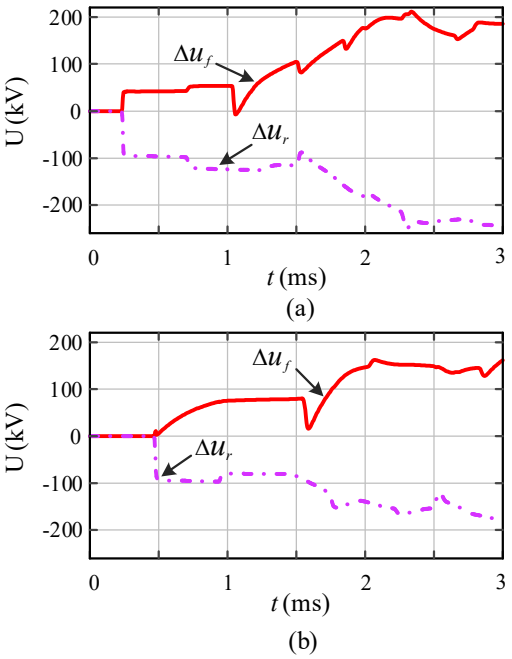


Fig. 8. Simulation of an internal fault on MN line. (a) TW detected by $R_1$; (b) TW detected by $R_2$.

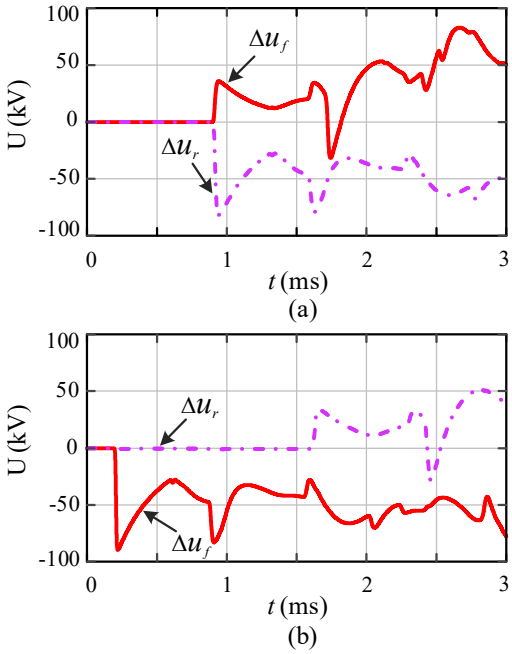


Fig. 9. Simulation of an external fault on NR line. (a) TW detected by $R_1$; (b) TW detected by $R_2$.

### C. *Performance of the Proposed Method*

#### 1) *Testing of Internal Faults on MN Line*

The fault resistance is 1 Ω, and the fault angle is 2°. At 80 kilometres from bus M, a phase A ground fault occurs at point $F_2$ on the MN line. The fault characteristics $NED_1$ for $R_1$ and $NED_2$ for $R_2$ are depicted in Fig. 10.

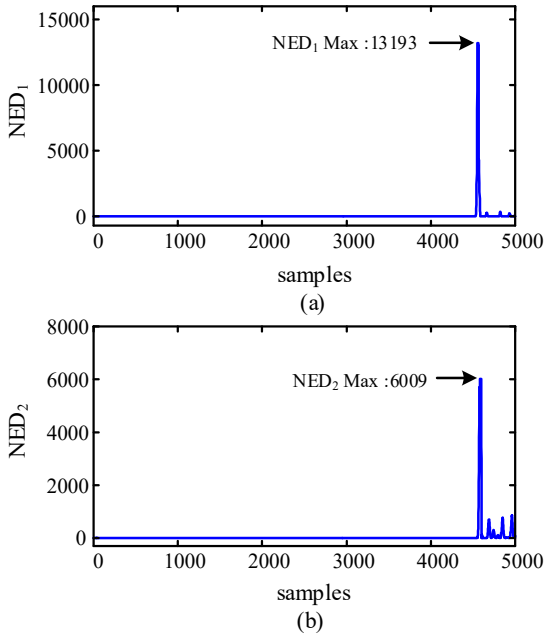


Fig. 10. Fault at point $F_2$, $R_f$ = 1 Ω, $\theta_f$ = 2°. (a) $NED_1$; (b) $NED_2$.

The maximum values of $NED_1$ and $NED_2$ for faults occurring at point $F_2$ under various fault angles and fault resistances are shown in Table I. Since $NED_1$ and $NED_2$ are periodic functions of the fault angle, Table I exclusively presents data for fault angles between 0° and 90° to conserve space.

As presented in Table I, for faults at $F_2$ with different fault resistances and fault angles, both $NED_1 > \lambda_{set}$ and $NED_2 > \lambda_{set}$. Therefore, both $R_1$ and $R_2$ identify the faults in the forward direction, confirming internal faults on the MN line.

TABLE I
TEST RESULTS OF POINT $F_2$ UNDER VARIOUS FAULT CONDITIONS.

| $\theta_f$(°) | $R_f$ (Ω) | | | | | |
|---|---|---|---|---|---|---|
| | 1 | 100 | 200 | 300 | 400 | 500 |
| | | | $NED_1$ | | | |
| 0 | 11806 | 15169 | 17692 | 19524 | 20769 | 25000 |
| 2 | 13193 | 18315 | 21868 | 24750 | 28696 | 23706 |
| 45 | 14034 | 19524 | 22553 | 24335 | 25348 | 25909 |
| 90 | 14335 | 20041 | 23146 | 24860 | 25837 | 26366 |
| | | | $NED_2$ | | | |
| 0 | 6097 | 7640 | 8718 | 9524 | 10769 | 12500 |
| 2 | 6009 | 7978 | 9467 | 10500 | 12174 | 13333 |
| 45 | 5781 | 7701 | 8707 | 9274 | 9589 | 9727 |
| 90 | 5892 | 7932 | 9001 | 9559 | 9874 | 10030 |

The fault resistance and fault angle are 5 Ω and 60°, respectively. The test results at various fault distances on the MN line are shown in Fig. 11.

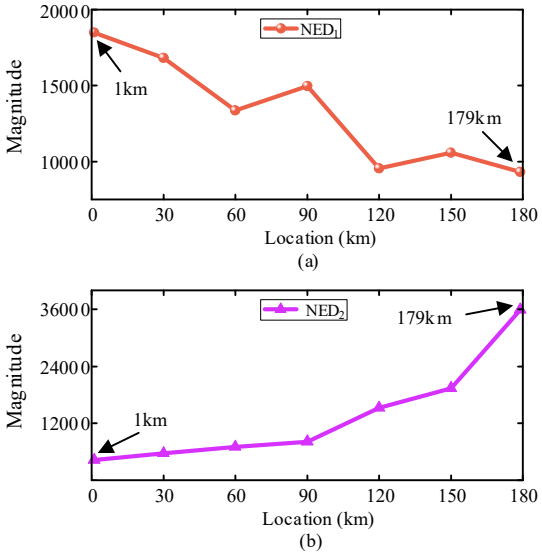


Fig. 11. Test results of various fault distances on MN line. (a) $NED_1$; (b) $NED_2$.

As shown in Fig. 11, both $R_1$ and $R_2$ correctly identify faults in the forward direction, i.e., $NED_1 > \lambda_{set}$ and $NED_2 > \lambda_{set}$. Therefore, the relays can accurately detect internal faults on the MN line without being affected by the fault distance.

*2) Testing of External Faults on LM Line*

The fault resistance is 1 Ω, and the fault angle is 2°. At 60 kilometres from bus L, a phase A ground fault occurs at point $F_1$ on the LM line. The fault characteristics $NED_1$ for $R_1$ and $NED_2$ for $R_2$ are shown in Fig. 12.

When faults occur at point $F_1$, under various fault resistance and fault angle conditions, the maximum values of $NED_1$ and $NED_2$ are depicted in Table II.

As presented in Table II, for faults at $F_1$ with various fault resistances and fault angles, where $NED_1 < \lambda_{set}$ and $NED_2 > \lambda_{set}$. Therefore, the relay correctly identifies them as external faults.

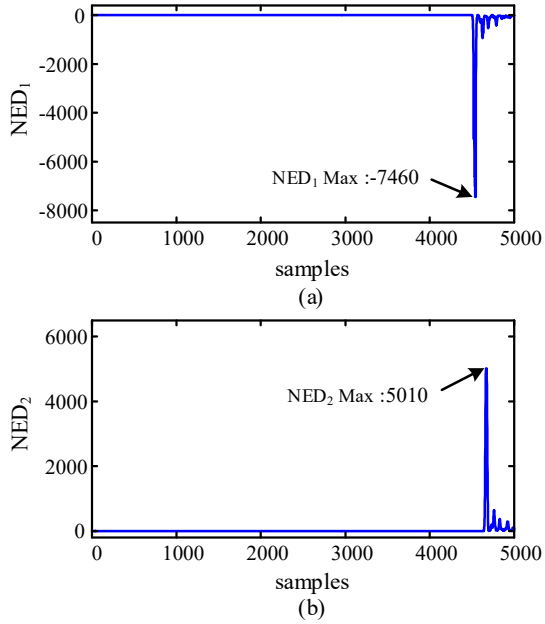


Fig. 12. Fault at point $F_1$, $R_f = 1$ Ω, $\theta_f = 2°$. (a) $NED_1$; (b) $NED_2$.

TABLE II
TEST RESULTS OF POINT $F_1$ UNDER VARIOUS FAULT CONDITIONS.

| $\theta_f$(°) | $R_f$ (Ω) | | | | | |
|---|---|---|---|---|---|---|
| | 1 | 100 | 200 | 300 | 400 | 500 |
| | | | $NED_1$ | | | |
| 0 | -7258 | -8202 | -9231 | -10000 | -10769 | -12500 |
| 2 | -7460 | -8876 | -9867 | -10750 | -12064 | -13334 |
| 45 | -8256 | -9682 | -10357 | -10706 | -10854 | -10864 |
| 90 | -8697 | -10279 | -11036 | -11389 | -11527 | -11562 |
| | | | $NED_2$ | | | |
| 0 | 4516 | 5056 | 5641 | 5714 | 6923 | 7500 |
| 2 | 5010 | 5669 | 6085 | 6404 | 6479 | 6809 |
| 45 | 5009 | 5542 | 5753 | 5868 | 5882 | 5880 |
| 90 | 4848 | 6168 | 5988 | 5554 | 5921 | 6036 |

The fault resistance and fault angle are 5 Ω and 60°, respectively. The test results at various fault distances on the LM line are presented in Fig. 13. As shown in Fig. 13, for faults occurring at any position on the LM line, $NED_1 < \lambda_{set}$ and $NED_2 > \lambda_{set}$. Therefore, the relays correctly identify them as external faults, unaffected by the fault distance.

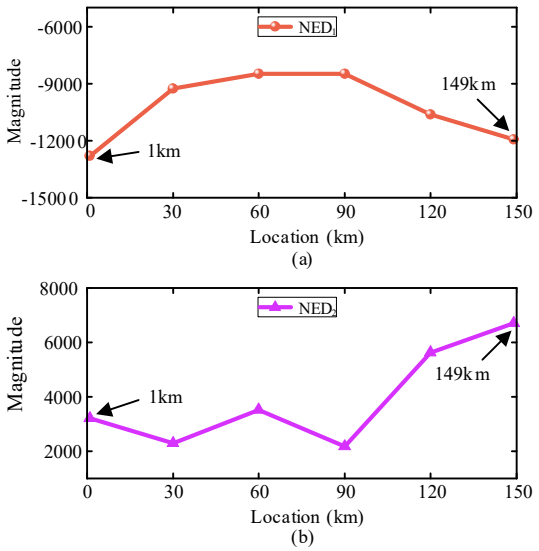


Fig. 13. Test results of various fault distances on LM line. (a) $NED_1$; (b) $NED_2$.

*3) Testing of External Faults on NR Line*

The fault resistance and the fault angle are 1 Ω and 2°, respectively. At 60 kilometres from bus N, a phase A ground fault occurs at point $F_3$ on the NR line. The fault characteristics $NED_1$ for $R_1$ and $NED_2$ for $R_2$ are shown in Fig. 14.

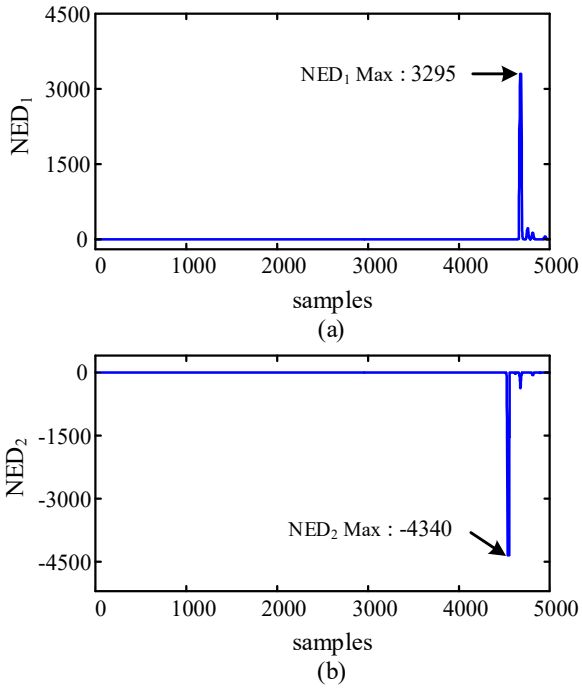


Fig. 14. Fault at point $F_3$, $R_f = 1$ Ω, $\theta_f = 2°$. (a) $NED_1$; (b) $NED_2$.

When faults occur at point $F_3$, under various fault resistance and fault angle conditions, the maximum values of $NED_1$ and $NED_2$ are depicted in Table III. As presented in Table III, for faults at $F_3$ with various fault resistances and fault angles, where $NED_1 > \lambda_{set}$ and $NED_2 < \lambda_{set}$. Therefore, the relay correctly identifies them as external faults.

The fault resistance and fault angle are 5 Ω and 60°, respectively. The test results at various fault distances on the NR line are shown in Fig. 15. As shown in Fig. 15, for faults occurring at any position on the NR line, $NED_1 > \lambda_{set}$ and $NED_2 < \lambda_{set}$. Consequently, the relays correctly recognise external faults, independent of the distance to the fault.

TABLE III
TEST RESULTS OF POINT $F_3$ UNDER VARIOUS FAULT CONDITIONS.

| $\theta_f$(°) | $R_f$ (Ω) | | | | | |
|---|---|---|---|---|---|---|
| | 1 | 100 | 200 | 300 | 400 | 500 |
| | | | $NED_1$ | | | |
| 0 | 2548 | 3146 | 3590 | 3810 | 4615 | 5000 |
| 2 | 3295 | 4551 | 5467 | 6000 | 6957 | 7333 |
| 45 | 3847 | 5714 | 6812 | 7480 | 7911 | 8091 |
| 90 | 4032 | 6126 | 7358 | 8077 | 8515 | 8769 |
| | | | $NED_2$ | | | |
| 0 | -3323 | -3933 | -4615 | -5238 | -5385 | -6250 |
| 2 | -4340 | -5955 | -7200 | -8000 | -9131 | -10002 |
| 45 | -6628 | -9951 | -11962 | -13206 | -13956 | -14455 |
| 90 | -7488 | -11490 | -13922 | -15381 | -16276 | -16817 |

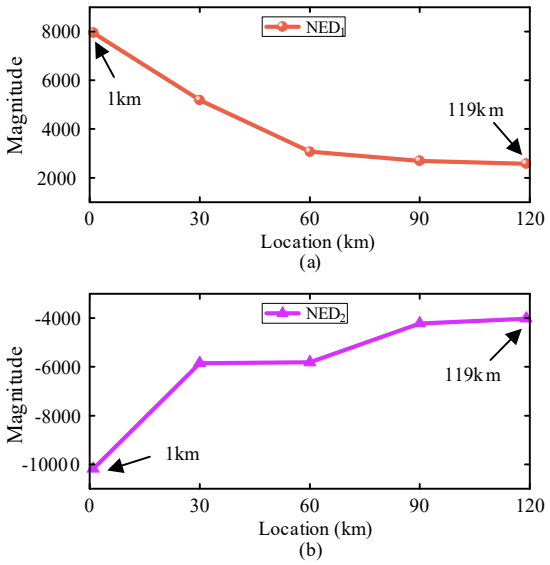


Fig. 15. Test results of various fault distances on NR line. (a) $NED_1$; (b) $NED_2$.

*4) Effect of Noise*

There are various interference signals present in the power grid, and noise is an unavoidable factor in the process of TW transmission. At operational sites, protective devices are susceptible to various types of noise interference, which may lead to erroneous actions or a lack of response from TW-based protections. In order to evaluate the performance of the protection under noisy conditions, white noise interference with a Signal-to-Noise Ratio of 25 dB is added to the sampled signals at different fault points. Fig. 16 illustrates the forward and reverse TWs at $F_3$, which is influenced by noise. The simulations for various fault conditions are listed in Table IV.

From the test results presented in Table IV, the amplitudes of $NED_1$ and $NED_2$ meet the protection criterion, even in the presence of 25 dB of sampling noise. $NED_1 > \lambda_{set}$ and $NED_2 < \lambda_{set}$, i.e., the faults at point $F_3$ are correctly identified as external faults. Consequently, it can be demonstrated that the sampling noise will not have an impact on the correctness of the proposed methodology.

*5) Effect of Source Impedance*

The above simulation establishes the system's source impedance at a fixed value. However, in practice, the operational mode of the power system may change at any

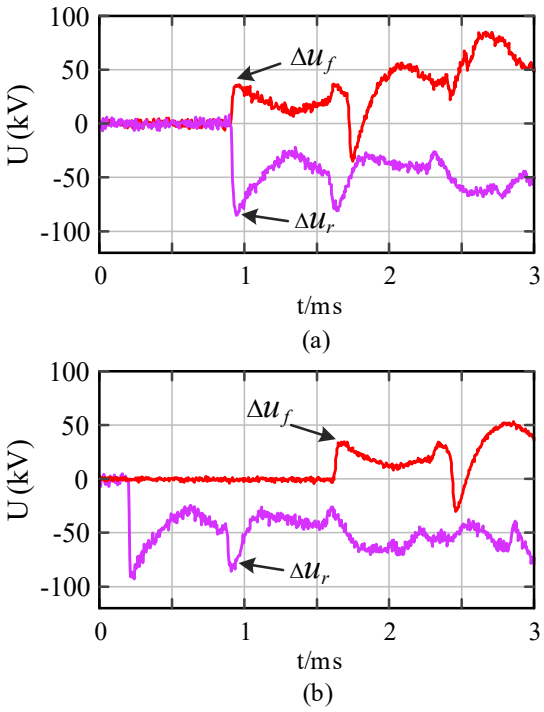


Fig. 16 The sampled signal is contaminated with 25dB of white noise at the $F_3$ point fault. (a) TW at $R_1$; (b) TW at $R_2$.

TABLE IV
TEST RESULTS AT POINT $F_3$ UNDER 25 DB WHITE NOISE INTERFERENCE.

| $\theta_f$(°) | $R_f$ (Ω) | | | | | |
|---|---|---|---|---|---|---|
| | 1 | 100 | 200 | 300 | 400 | 500 |
| | | | $NED_1$ | | | |
| 0 | 2943 | 3407 | 3781 | 4006 | 4794 | 5401 |
| 2 | 3465 | 4762 | 5490 | 5979 | 7169 | 7642 |
| 45 | 4197 | 5894 | 7211 | 7688 | 8138 | 8125 |
| 90 | 4558 | 6433 | 7643 | 8342 | 8637 | 9267 |
| | | | $NED_2$ | | | |
| 0 | -3742 | -4138 | -4832 | -5691 | -5749 | -6358 |
| 2 | -4628 | -6296 | -7516 | -8364 | -9769 | -10422 |
| 45 | -6837 | -11070 | -12650 | -14656 | -14201 | -14295 |
| 90 | -7655 | -13041 | -14584 | -15477 | -17620 | -17443 |

TABLE V
TEST RESULTS AT DIFFERENT SOURCE IMPEDANCES.

| source impedance ($S_2$) | Location | $NED_1$ | $NED_2$ | Analysis Result |
|---|---|---|---|---|
| 50% | $F_1$ | -11279 | 6517 | External |
| | $F_2$ | 24860 | 10038 | Internal |
| | $F_3$ | 6369 | -8390 | External |
| 100% | $F_1$ | -10750 | 6404 | External |
| | $F_2$ | 24750 | 10500 | Internal |
| | $F_3$ | 6000 | -8000 | External |
| 200% | $F_1$ | -9743 | 6035 | External |
| | $F_2$ | 18711 | 9762 | Internal |
| | $F_3$ | 5840 | -7592 | External |
| 300% | $F_1$ | -9579 | 6148 | External |
| | $F_2$ | 18420 | 9439 | Internal |
| | $F_3$ | 5736 | -7622 | External |

time. To evaluate the performance of the proposed protection under varying operational modes of the system, simulations were conducted while keeping all other conditions constant and altering the impedance value of the equivalent source $S_2$. On the basis of the parameters given in Section 6.1, the value of the source impedance is varied from 50% to 300%. The

fault angle and fault resistance are consistently set at 300 Ω and 2°, respectively. The simulation results for phase A ground faults are presented in Table V.

After altering the equivalent source impedance, the simulation data presented in Table V demonstrates that the fault direction can still be correctly identified based on the magnitudes of $NED_1$ and $NED_2$. The results confirms that the proposed method is unaffected by changes in the system's operating mode.

*6) Operation Time Analysis*

The operating time of the protection is comprehensively influenced by the data window $d$, the execution time of the algorithm and the communication time. $T_a$ is defined to be the time required from the appearance of the fault to the protection action, as defined in (28).

$$T_a = d + T_1 + T_2 \tag{28}$$

wherer $T_1$ represents the time required to execute the algorithm, and $T_2$ denotes the time taken for signal communication. The data window $d$ is equal to $2l_{min}/v$, and for general EHV transmission systems, $d$ is less than 2.5 ms. The execution time of the algorithm is predominantly consumed by the Karenbauer phase-mode transform (27) and the S-transform (20), which nearly encompass 1497300 equivalent additions. The typical DSP chip has a computing power of more than 100 million instructions per second and can complete the computational task of the algorithm within 1.5 ms. Considering that the delay in an fiber optic communication system is approximately 4.8 microseconds per kilometer, the communication time for the normal EHV systems is less than 2 ms.

In conclusion, the proposed approach can signal the action of the protection device within 6 ms. Consequently, the high-speed TW protection will respond rapidly when a fault is detected in the transmission line.

*7) Comparison with Existing Methods*

To demonstrate the superiority of the proposed approach, we compared it with several existing methods from multiple perspectives, as shown in Table VI.

TABLE VI
A COMPARISON OF VARIOUS PROTECTION METHODS.

| Indexes | [5] | [7] | [14] | This paper |
|---|---|---|---|---|
| Sampling rate (kHz) | 1000 | 1000 | 400 | 200 |
| Rule-based | ✓ | ✓ | × | ✓ |
| fault angle = 0° | × | × | × | ✓ |
| Maximum fault resistance (Ω) | 200 | 400 | 300 | 500 |
| Immune to noise | ✓ | N | N | ✓ |
| Immune to source impedance | N | N | N | ✓ |

Note: N denotes not researched or reported.

The conclusions can be drawn from the results presented above: 1) Compared with the methods in [5], [7], and [14], the proposed algorithm requires only a 200 kHz sampling rate, which greatly reduces the hardware costs. 2) Other methods exhibit a lack of reliability and low sensitivity at small fault angles and high fault resistances. In contrast, the method presented in this paper incorporates fault factors into the fault characteristics, making it robust against variations in fault angles and fault resistances. 3) The proposed approach is independent of noise and variations in source impedance, and it demonstrates high reliability.

## VII. CONCLUSION

In this paper, a TW directional pilot protection considering fault factors is proposed. Firstly, this paper investigates the differences in directional TW energy during faults, establishing the fundamental principles of directional discrimination of relay. Secondly, based on simulation and analysis, this paper demonstrates the necessity for considering fault factors in fault discrimination. Subsequently, the protection algorithm considering fault factors is proposed, which normalizes the fault characteristics to the same fault condition. Finally, based on the engineering parameters of the Central China Power Grid, a simulation system is constructed in EMTP-RV. Extensive test results demonstrate that the proposed method can swiftly and reliably determine fault directions under various fault conditions. Compared to conventional protection schemes, the proposed approach offers the following advantages:

1) The normalized fault characteristic includes fault resistance and fault angle information, eliminating the influence of these two fault factors.

2) The S-transform effectively extracts the information of fault-generated TW.

3) Capable of reliably identifying faults under weak fault conditions.

## REFERENCES


[1] F. Xie, Z. Hao, D. Ye, S. Yang, C. Li, G. Dai, B. Zhang, and T. Wang, "A non-unit line protection method for MMC-HVDC grids based on the curvatures of backward traveling waves," International Journal of Electrical Power & Energy Systems, vol. 153, pp. 109373, 2023

[2] F. Kong, Z. Hao, and B. Zhang, "A Novel Traveling-Wave-Based Main Protection Scheme for ±800 kV UHVDC Bipolar Transmission Lines," Ieee Transactions on Power Delivery, vol. 31, no. 5, pp. 2159-2168, 2016

[3] D. Mu, S. Lin, H. Zhang, and T. Zheng, "A Novel Fault Identification Method for HVDC Converter Station Section Based on Energy Relative Entropy," Ieee Transactions on Instrumentation and Measurement, vol. 71, pp. 1-10, 2022

[4] L. Tang, X. Dong, S. Luo, S. Shi, and B. Wang, "A New Differential Protection of Transmission Line Based on Equivalent Travelling Wave," Ieee Transactions on Power Delivery, vol. 32, no. 3, pp. 1359-1369, 2017

[5] R. Liang, Z. Wang, N. Peng, F. Zare, X. Liu, and C. Liu, "Traveling wave protection based on asynchronously sampled time difference of arrival of modulus traveling waves in per unit line length," Electric Power Systems Research, vol. 165, pp. 250-258, 2018

[6] J. Wang, and Y. Zhang, "Traveling Wave Propagation Characteristic-Based LCC-MMC Hybrid HVDC Transmission Line Fault Location Method," Ieee Transactions on Power Delivery, vol. 37, no. 1, pp. 208-218, 2022

[7] F. Namdari, and M. Salehi, "High-Speed Protection Scheme Based on Initial Current Traveling Wave for Transmission Lines Employing Mathematical Morphology," Ieee Transactions on Power Delivery, vol. 32, no. 1, pp. 246-253, 2017

[8] H. Wu, X. Dong, and R. Ye, "A new algorithm for busbar protection based on the comparison of initial traveling wave power," Ieej Transactions on Electrical and Electronic Engineering, vol. 14, no. 4, pp. 520-533, 2019

[9] A. Y. Lei, X. Z. Dong, and V. Terzija, "An Ultra-High-Speed Directional Relay Based on Correlation of Incremental Quantities," Ieee Transactions on Power Delivery, vol. 33, no. 6, pp. 2726-2735, 2018

[10] Z. Y. He, X. M. Liu, X. P. Li, and R. K. Mai, "A Novel Traveling-Wave Directional Relay Based on Apparent Surge Impedance," Ieee Transactions on Power Delivery, vol. 30, no. 3, pp. 1153-1161, 2015

[11] Y. Kong, B. H. Zhang, and Z. G. Hao, "Study of Ultra-High-Speed Protection of Transmission Lines Using a Directional Comparison Scheme of Transient Energy," Ieee Transactions on Power Delivery, vol. 30, no. 3, pp. 1317-1322, 2015

[12] H. Li, J. D. Duan, Y. Lei, and L. H. Tuo, "Ultra-high-speed transient-based directional relay for AC transmission lines connected to LCC-HVDC inverter station," International Journal of Electrical Power & Energy Systems, vol. 123, pp. 13, 2020
[13] Z. Guo, J. Yao, S. Yang, H. Zhang, T. Mao, and D. Thanh Long, "A new method for non-unit protection of power transmission lines based on fault resistance and fault angle reduction," International Journal of Electrical Power & Energy Systems, vol. 55, pp. 760-769, 2014
[14] Z. Guo, J. Yao, Y. Jiang, X. Zhu, Z. Tan, and W. Wen, "A novel distributed unit transient protection algorithm using support vector machines," Electric Power Systems Research, vol. 123, pp. 13-20, 2015
[15] X. Xu, "Research on a Small Target Object Detection Algorithm for Electric Transmission Lines Based on Convolutional Neural Network," IAENG International Journal of Computer Science, vol. 50, no. 2, pp. 375-380, 2023
[16] J.-C. Wan, "Fast Risk Estimation through Fourier Transform Based Multilevel Monte Carlo Simulation," IAENG International Journal of Applied Mathematics, vol. 54, no. 4, pp. 730-741, 2024
[17] M. Lashgari, and S. M. Shahrtash, "Ultra-fast busbar protection employing fast S transform of current signals," International Journal of Electrical Power & Energy Systems, vol. 114, pp. 9, 2020
[18] G. N. Lopes, T. S. Menezes, G. G. Santos, L. Trondoli, and J. C. M. Vieira, "High Impedance Fault detection based on harmonic energy variation via S-transform," International Journal of Electrical Power & Energy Systems, vol. 136, pp. 12, 2022
[19] H. Wu, J. Yang, L. Chen, and Q. Wang, "A new method for identifying a fault in T-connected lines based on multiscale S-transform energy entropy and an extreme learning machine," Plos One, vol. 14, no. 8, 2019
[20] L. Gelman, and T. H. Patel, "Novel intelligent data processing technology, based on nonstationary nonlinear wavelet bispectrum, for vibration fault diagnosis," IAENG International Journal of Computer Science, vol. 50, no. 1, pp. 1-6, 2023
[21] W. Zhang, and D. Wang, "S-Transform Based Traveling Wave Directional Pilot Protection for Hybrid LCC-MMC-HVDC Transmission Line," Energies, vol. 15, no. 13, 2022
[22] H. Miyajima, N. Shigei, H. Miyajima, and N. Shiratori, "Securely Distributed Computation with Divided Data for Particle Swarm Optimization." Lecture Notes in Engineering and Computer Science: Proceedings of the International MultiConference of Engineers and Computer Scientists 2021, 20-22 October, 2021, Hong Kong, pp. 1-6
[23] J. Doria-Garcia, C. Orozco-Henao, L. U. Iurinic, and J. Diego Pulgarin-Rivera, "High impedance fault location: Generalized extension for ground faults," International Journal of Electrical Power & Energy Systems, vol. 114, 2020
[24] B. Xia, Y. Wang, E. Vazquez, W. Xu, D. Wong, and M. Tong, "Estimation of Fault Resistance Using Fault Record Data," Ieee Transactions on Power Delivery, vol. 30, no. 1, pp. 153-160, 2015
[25] Yin-Yin Bao, Yu Liu, Jie-Sheng Wang, and Ming-Wei Wang, "GMDH-type Neural Network Based Short-term Load Forecasting Method in Power System," IAENG International Journal of Computer Science, vol. 50, no.4, pp1194-1201, 2023